Background problem in electron-energy-loss spectroscopy

D. S. Su and E. Zeitler
Fritz-Haber-Institut der Max-Planck-Gesellschaft, Faradayweg 4-6, W-1000 Berlin 33, Germany
(Received 30 November 1992)

At large scattering angle the background formation in electron-energy-loss spectroscopy is determined by elastic-inelastic scattering events. The suitability of the usual background fitting AE^{-r} is critically investigated as a function of specimen thickness, collection angle, and width of energy window.

I. INTRODUCTION

Electron-energy-loss spectroscopy (EELS) combined with electron microscopy has become a powerful tool in materials science and biology. Fundamental excitations of electrons in the bulk, on the surface, or at interfaces or transitions in the bands permit the study of the electric and dielectric properties of the specimen.[1,2] Detection of the characteristic excitation of inner-shell electrons by EELS affords the determination of the elemental composition of a specimen.[3] In the meantime, imaging energy filters allow one to produce elemental maps and energy-selected diffraction patterns.[4,5] Equally interesting is the determination of momentum distribution of atomic electrons by EELS measurements of Compton profiles.[6]

However, all these applications of EELS face the so-called background problem, i.e., the proper subtraction of the large numbers without infringing on the weak signal.[2] The preedge background results from all possible scattering processes whose energy is less than the edge energy and the combination of all these processes, including multiple scattering and channeling of different scattering events. The final distribution of energy and angle of electrons is then determined by complicated impact processes of incident electrons in the specimen. From an experimental standpoint, additional contributions to the background may exist due to spurious scattering of electrons into the spectrometer or due to detector noise.

Studies of the background problem in EELS can be divided into two kinds. One performs a numerical fitting of the measurements before the edge and extrapolates the result as background beyond the edge region. The contribution of the inner-shell excitation riding on the background is obtained by subtracting from the measured spectrum the extrapolated background. Usually an expression AE^{-r} is assumed, whose two free parameters A and r are determined by least-squares methods or by the two-area method.[2,7,8] But it is found that the power-law index r is strongly dependent on experimental parameters like collection aperture, specimen thickness, and width and location of the energy window. This is the main reason that EELS microanalysis is critical and inaccurate.

The second approach is the simulation of the physical events in order to understand the influence of the crucial parameters and thus to find the optimal conditions for the experiment. Along this line Rez[9] calculated the effect of multiple scattering on the shape of the edge, albeit by using a rather crude approximation of the inelastic cross section. This work made plausible how the slope of the spectrum changes and how the edge softens as the specimen thickness increases. Similar results were derived by Leapman and Swit[10] using a self-convolution method. The dependence of the background and its slope on the collection angle, which is a very significant parameter for the detection quality, was, however, not investigated.

It was Jouffrey *et al.* who dealt with this problem. They used, for computing the energy-loss spectrum, experimentally determined parameters for the electron-sample interaction.[11] With this method they successfully simulated the entire energy-loss spectrum for carbon and calculated the jump ratio (defined as the ratio between the maximum of the characteristic loss and the background) for aluminum as a function of specimen thickness. Simulations have been performed also for gases at different pressures in an environmental cell adapted to a 1-MeV microscope: the calculations are in rather good agreement with experiments.

The simplicity of the Jouffrey *et al.* method stems from the assumption that the number of electrons that scatter into the collection aperture after n events is equal to the nth power of those electrons which scatter singly into the aperture. The validity of this crucial assumption was investigated by Egerton and Wang[12] and further by Su,[13] especially with regard to the deconvolution of energy-loss spectra recorded with an angle-limiting aperture.[14] But their approaches still suffered from the critical simplification of separating the scattering probability into a product of two functions, one depending on the energy loss and the other on the scattering angle.

It is the goal of this paper to present a formulation of the EELS background that takes into account the proper energy loss and angle distribution of all types of scattering events to any order of multiplicity without resorting to unrealistic simplifications. Such a formulation gives considerable insight into the nature of the background; it also gives more accurate and reliable numerical results than the previous theories albeit by greater mathematical and hence computational effort. A detailed test indeed confirms the inadequacy of the crude power-law model of the background.

II. FORMULATION OF THE PROBLEM

We extend the formulation by Crewe and Groves[15] of multiple small-angle electron scattering in a homogeneous target to account for m different types (channels) of

0163-1829/93/47(22)/14734(7)/$06.00

energy-loss mechanisms (e.g., plasmon losses, various inner-shell losses, etc.). As the mean number of scattering events of the various types of interaction j differs according to the particular cross section σ_j, we measure the specimen thickness t in units of the mean free pathlength λ_j, introducing the *mean* number $D_j = t/\lambda_j$ and the actual number n_j of the occurrence.

The probability for the combined event $\mathbf{n}=\{n_1,n_2,n_3 \cdots n_m\}$ to occur when the experimental setting is $\mathbf{D}=\{D_1,D_2,D_3,\ldots,D_m\}$ becomes, according to Poisson,

$$P_{\mathbf{n}} = e^{-D} \prod_1^m \left[\frac{D_j^{n_j}}{n_j!} \right] , \tag{1}$$

where we introduced the *total* mean number of events as

$$D = \frac{t}{\lambda} = \sum_{i=1}^{m} D_i = t \sum_{i=1}^{m} \frac{1}{\lambda_i} \tag{2}$$

counting all possible types of interaction.

The total distribution $F_{\mathbf{n}}(E,\boldsymbol{\theta})$ for $\mathbf{n}$ events results from multiple convolutions in energy loss and angle of the various partial distributions

$$f_j * f_k = \int_0^E d\epsilon \int_\Omega d\boldsymbol{\beta} f_j(\epsilon,\boldsymbol{\beta}) f_k(E-\epsilon,\boldsymbol{\theta}-\boldsymbol{\beta}) \tag{3}$$

and can be written as

$$F_{\mathbf{n}} = f_1^{*n_1} * \cdots * f_2^{*n_1} * \cdots * f_m^{*n_m} , \tag{4}$$

where we express the k-fold convolution operation as f^{*k}.

The distribution of the electrons that suffered in the layer a total energy loss E and by scattering a total deviation $\boldsymbol{\theta}$ from the incident direction is

$$P(E,\boldsymbol{\theta}) = \sum_{\mathbf{n}} P_{\mathbf{n}} F_{\mathbf{n}}(E,\boldsymbol{\theta}) . \tag{5}$$

Since the required convolutions are most readily performed by a detour through Fourier space, we introduce the energy and momentum transform, denoted by a tilde,

$$\mathcal{F}[g] = \tilde{g}(\omega,\boldsymbol{\rho}) = \int_0^\infty \int_\Omega g(E,\boldsymbol{\theta}) e^{-i(E\omega+\boldsymbol{\theta}\cdot\boldsymbol{\rho})} dE\, d\boldsymbol{\theta} . \tag{6}$$

Applying the Fourier transform and using the convolution theorem, we get in Fourier space the simple expression

$$\tilde{P}(\omega,\boldsymbol{\rho}) = e^{-D} e^{(D_1\tilde{f}_1 + D_2\tilde{f}_2 + \cdots + D_m\tilde{f}_m)} . \tag{7}$$

If we let

$$\begin{aligned} \tilde{f}(\omega,\boldsymbol{\rho}) &= \lambda \left[\frac{1}{\lambda_1}\tilde{f}_1 + \frac{1}{\lambda_2}\tilde{f}_2 + \cdots + \frac{1}{\lambda_m}\tilde{f}_m \right] \\ &= \lambda \sum_{i=1}^{m} \frac{1}{\lambda_i}\tilde{f}_i \end{aligned} \tag{8}$$

be the distribution of a fictitious single event weighted and averaged properly over all possible events, then we have

$$\tilde{P}(\omega,\boldsymbol{\rho}) = e^{D[\tilde{f}(\omega,\boldsymbol{\rho})-1]} . \tag{9}$$

The task is finished by taking the inverse Fourier transform; in short, the whole procedure can be expressed as

$$P(E,\boldsymbol{\theta}) = \mathcal{F}^{-1}[e^{D(\mathcal{F}[f(E,\boldsymbol{\theta})]-1)}] . \tag{10}$$

Equation (10), incidentally, is also the solution of the transport equation.[16] This result has been applied to the study of straggling, that is, for multiple energy loss. Most dominant is the early work by Landau,[17] followed by Blunck and Leisegang,[18] and Vavilov;[19] more pertinent to the contrast and resolution in the electron microscope are the papers by Groves,[21] Reimer,[16] and Rez.[20]

III. SPECIFICATION OF THE PROBLEM

Although the general formalism is developed in the previous section, we would like to adapt it to the problem at hand by slight modification, thereby gaining additional physical insights. From an experimental point of view we have four types of scattering channels whose relative importance changes with specimen thickness but also with the angle of observation. In other words the mean impact numbers for the various types, and hence the composition of the total distribution, change with the parameters mentioned. Thus, the most frequent type of interaction will characterize the overall behavior.

In analytical EELS the four types of electron-scattering channels can be discerned quite readily (note lower indices).

The unscattered distribution $f_0 = \delta(E)\delta(\theta)$. It retains the primary energy distribution of the source and the angular distribution of the incident electrons. We suppose here a monoenergic and parallel incident beam.

Elastically scattered electrons $f_1(\theta)\delta(E)$. They are scattered by atomic nuclei and by phonons. The energy loss by phonons is very small (less than 0.1 eV) and below the energy resolution of EELS (larger than 1 eV); therefore the scattering is usually accepted as a quasielastic event.

Low-energy-loss electrons $f_2(E,\theta)$. They suffer relatively low-energy losses leading to band and plasmon excitations. Also, the energy losses resulting from inner-shell excitation with an energy loss less than 100 eV belong to this category.

High-energy-loss electrons $f_3(E,\theta)$. They interact with, for instance, K-shell electrons of atoms. They can also suffer Compton scattering by transferring large amounts of energy and momentum to the single-valence electrons.

For our purpose it is important to emphasize the influence of the elastically scattered electrons on the energy-loss spectrum. This seems contradictory since elastic scattering does not generate any energy loss. But energy loss is accompanied by an elastic-inelastic channeling. It is the change in the angular distribution which brings about a change in the finite collection efficiency.

After dividing the scattering into the types mentioned, the final equation consists only of four factors:

$$\tilde{P} = e^{-D} \tilde{W}_1 \tilde{W}_2 \tilde{W}_3 . \tag{11}$$

To highlight the action of elastic scattering we separate

each factor $\tilde{W}_i = 1 + \tilde{P}_i$ into the unscattered and scattered parts so that we obtain

$$\tilde{P} = e^{-D}([\tilde{P}_2 + \tilde{P}_3 + \tilde{P}_2\tilde{P}_3] + \tilde{P}_1[\tilde{P}_2 + \tilde{P}_3 + \tilde{P}_2\tilde{P}_3] + 1 + \tilde{P}_1) . \quad (12)$$

The result is quite simple: in the square brackets we have the proper combinations of all exclusively inelastically scattered electrons, and this combination is multiplied in the next term by the elastic scattering factor $\tilde{P}_1$. The last term expresses the part without energy loss, i.e., the unscattered and the elastically scattered components. This separation shows clearly the error that will be committed when elastic scattering is neglected. In real space all inelastic scattering must be convoluted with the elastic distribution. In order to appreciate the significance of this channeling of elastic-inelastic events, we discuss the various terms in Eq. (12) separately.

The term $e^{-D}\tilde{P}_1$ expresses the multiple elastic scattering of electrons after the layer t. This has been treated by Keil, Zeitler, and Zinn.[22] In the case of angle-resolved EEL spectra, the intensity from this scattering will be recorded in the channel of $E = 0$ and will be used for the further processing of the measured spectra.[23,24]

The terms $e^{-D}\tilde{P}_2$ and $e^{-D}\tilde{P}_3$ give, after inverse Fourier transformation, the energy and angular distribution of multiple low-energy-loss and high-energy-loss scattered electrons, without any channel crosstalk. The term $e^{-D}\tilde{P}_2\tilde{P}_3$ couples the lower-energy-loss channel with the higher-energy-loss channel. This gives an intensity contribution to the characteristic edge which is superpositioned on $e^{-D}\tilde{P}_3$. If the characteristic edge is at E_{edge}, this contribution shows a maximum displaced from the edge to, for instance, $E_{\text{edge}} + E_{\text{plasma}}$, if one *plasmon event* followed the *edge event*. So this term does not contribute to the *pre*edge background. This channeling can also be coupled with the elastic channel, as expressed by $e^{-D}\tilde{P}_1\tilde{P}_2\tilde{P}_3$. This additional intensity can be canceled with the routine Fourier ratio deconvolution[2] for microanalysis. Finally, $e^{-D}\tilde{P}_1\tilde{P}_2$ and $e^{-D}\tilde{P}_1\tilde{P}_3$ describe the elastic-inelastic channeling processes, but without spectral displacements since no additional energy losses accompany the elastic event.

IV. RECONSTRUCTION OF SINGLE-SCATTERING DISTRIBUTION AND NUMERICS

The first step in this study is then to select the single-event distribution function $f_i(E,\theta)$. Since the method discussed is independent of this selection, different physical models of the scattering process may be used depending on interest and purpose. In order to show the advantage of the method and to convey at the same time a physical understanding of the background in EELS, numerical calculations are carried out for aluminum under usual experimental conditions. Also, the cross sections stem from standard models.

The L-shell distribution is derived from a hydrogenic model, whereas a free-electron gas model describes the plasmon excitation and Compton scattering. Dispersion and damping parameters are taken from experiment.[25] A simple Lenz formula[26] describes the elastic scattering which, in turn, is calibrated by adjusting the different parameters λ_i in Eq. (9) in accord with experiments.[16,27] The primary energy is 100 kV.

A standard fast-Fourier transform (FFT) is used for the energy transform. On account of symmetry, the two-dimensional Fourier transform with respect to the solid angle reduces to a Hankel transform of zero order:[28]

$$\tilde{g}(\omega,\rho) = \int_0^\infty \int_0^\infty g(E,\theta) e^{-iE\omega} J_0(\theta\rho) dE\,\theta\,d\theta , \quad (13)$$

where J_0 is the Bessel function of the first kind. A newly developed algorithm for discrete Hankel transforms,[29] which has been successfully used in the earlier works concerning electron scattering,[13,30–32] can be used for angular transform. An alternative algorithm, namely, the projected-functions method of Misell and Burge[33] and of Reimer,[16] is used in the present work.

Now one may argue that it should not be necessary to take n-fold multiple scattering into account as we have done thus far. The tenfold multiple scattering, for instance, would not be interesting because its probability is almost zero (due to the Poisson distribution) and/or the resulting energy loss overshoots the region of interest. Surely some simplification could be achieved, but the multiple-scattering effects become more serious as thickness increases and the scattering events of one electron happen, on average, more than twice. In fact, it is the advantage of our method that we can consider *all* multiple scattering without any numerical problems. On the contrary, if one takes the multiple scattering into account only up to n-fold, the beautifully simple formula (7) or (9) must be replaced by summations of n terms. Hence we forgo any simplification and truncation, and retain the ease and accuracy of the calculation.

V. RESULTS AND DISCUSSION

All energy-sensitive detector systems possess a finite angular acceptance. If this acceptance is dependent on the setting up of the energy window, the recorded spectra are a complicated composite. Let us clarify the situation by discussing the various energy-loss ranges in which special interactions dominate, such as the plasma losses in the low range and the inner-shell excitations and Compton scattering at higher losses. This distinction is justified since the angular width of the inelastic scattering grows linearly with the energy loss, whereas the width of the elastic scattering distribution stays constant. In other words, the influence of the elastic scattering on the accuracy of measured spectra, which is the topic of this paper, is not at all constant. Full appreciation can be derived from the following discussion of angle-resolved EELS.

A. Angle-resolved EELS with low-energy loss

In this region plasma losses are the most frequent events. Depending on the sample thickness, multiple plasma losses can occur, but for all practical purposes samples showing more than threefold losses are too thick for accurate studies. In Fig. 1, energy-loss spectra of an

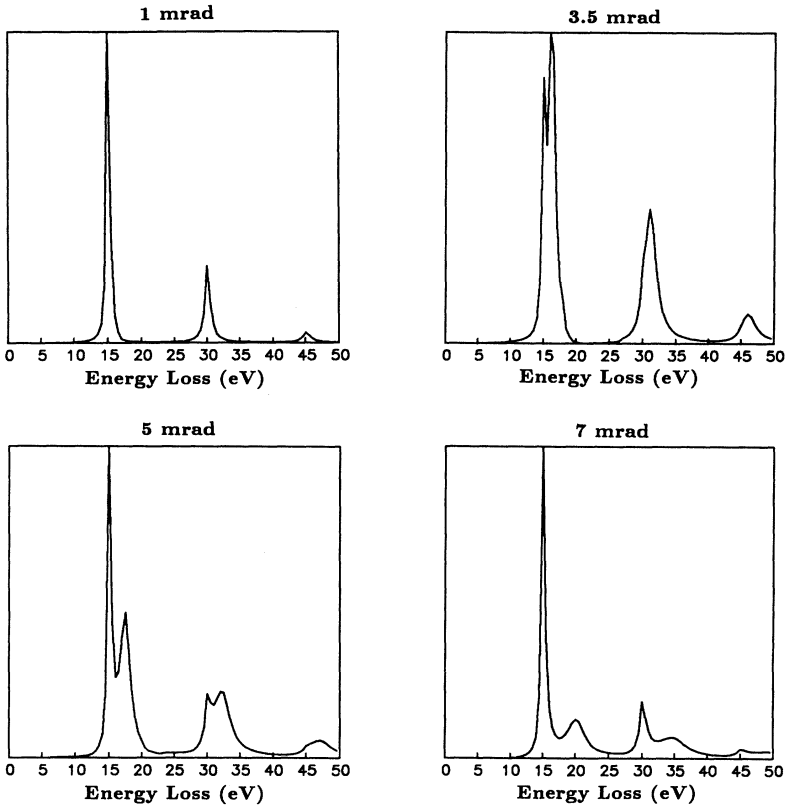

FIG. 1. Angle-resolved plasmon spectra for $D_2=0.5$.

Al sample are shown for a sequence of observation angles. The thickness of the sample is one-half free pathlength relative to the plasmon free pathlength which at 100-kV primary energy translates into 3.11×10^{-5} g/cm^2 or 115 nm. At 1-mrad observation angle, three sharp peaks with relative heights 100, 24, and 3 can clearly be seen as expected, in agreement with the Poisson distribution. At higher angles the single plasma loss occurs at higher energies. A quadratic relation between angle and energy loss exists as well-known dispersion. But another phenomenon becomes evident: the splitting of the peaks into two, the higher one remaining at the undispersed plasma loss, the second one shifting. This is the influence of elastic scattering. Let us use the formulas as guide for this discussion. The term $e^{-D}P_2$ contains all single, double, and multiple plasma losses; the other term $e^{-D}P_1P_2$ refers to electrons which not only suffered plasma losses but also have undergone single, double, or multiple elastic deviations from their path. Since the width of the angular plasmon distribution is only about one-hundreth of that of the elastic scattering distribution, it acts in the required convolution like a δ function. Thus, the dispersion of the plasmon cannot become effective. The resulting mixture of elastic- and plasmon-scattered electrons appears at the unshifted multiple-plasmon loss energy, whereas the electrons with only plasma losses show strongly dispersing broadened loss peaks.

Considering the various curves in Fig. 1 as sections through a three-dimensional (3D) plot of the intensity versus energy loss and angle, one obtains a clear picture of the situation and also a caveat when fine structures of energy-loss peaks are to be explained. These additional peaks form an unexpected background which, however, can be eliminated readily in Fourier space by division $\tilde{P}/(1+\tilde{P}_1)$.[31]

B. Angle-resolved spectrum with high-energy loss

The main application of angle-resolved EELS in the high-energy-loss region is the measure of the large-angle Compton scattering of electrons. This technique, known as ECOSS (electron Compton scattering of solids), gives a direct measurement of momentum distribution of valence electrons.[6,34] In Fig. 2, we show the single-loss distribution at large scattering angle. The Bethe ridge is clearly seen; it is formed by L-shell and valence electron scattering. The profile of the ridge shows the two contributions distinctly separated into a flat extended region and a sharply delineated parabola, whose intersection with the underground is marked by the abrupt change in slope. From a physical point of view these points of intersection relate to the Fermi momentum of the metallic *sp* sample.[35]

Experimentally, however, the Bethe ridge is drowned by multiple scattering depending on energy loss and scattering angle (Fig. 3). Because of the very narrow angular distribution and low-energy loss (15 eV) of plasma scattering, the probability that an electron will be scattered onto this Bethe ridge at some hundred eV solely via plasmon events is therefore negligible. The same is true for the slightly higher L-shape electron excitation (73 eV). However, due to the large cross section for plasmon

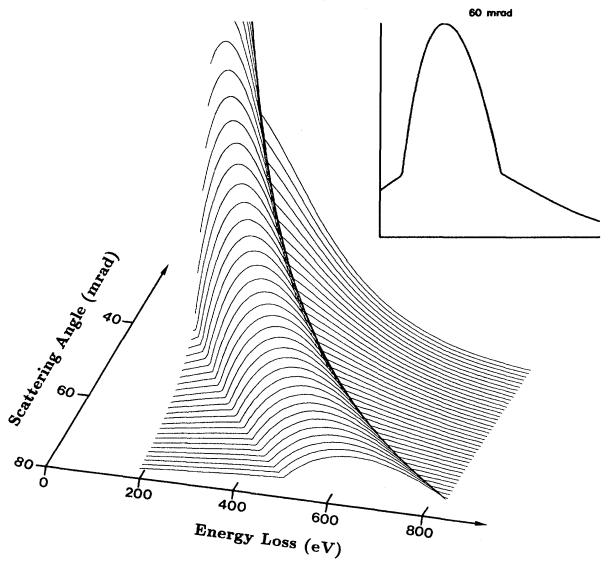

FIG. 2. Single-loss distribution at large scattering angle and high-energy loss.

scattering in aluminum (and also in most other light elements), the coupled scattering events, i.e., one plasmon event followed by Compton scattering, become more important. But this channeling results in only a shift of the Compton peaks to higher energies and a suppression of the abrupt change of the Compton profiles slope. This smoothing causes a decrease in energy resolution. Hence the strong background in Fig. 3 stems only from elastic-inelastic events. One of the Compton profiles is shown in the inset in Fig. 3, together with the background calculated from the elastic-inelastic channeling.

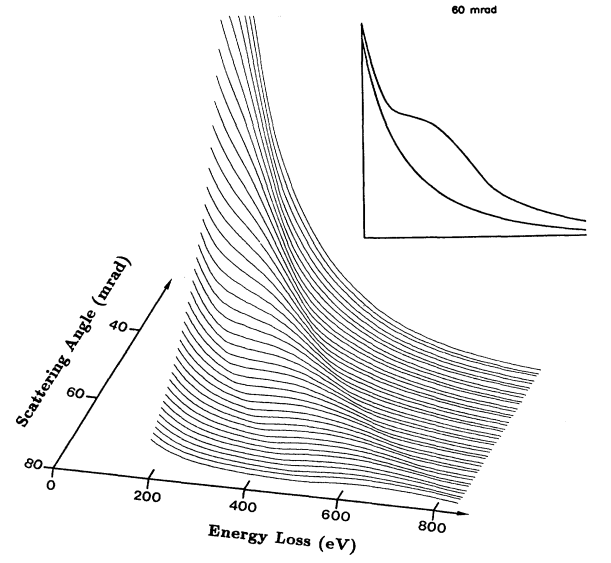

FIG. 3. Final energy and angular distribution after multiple scattering and channel coupling ($D_2=1$). The inset shows one Compton profile at 60-mrad scattering angle, together with the background calculated from elastic-inelastic channeling.

Unlike in plasmon spectra where the elastic-inelastic channeling results in a sum of single peaks located at multiples of the single plasmon energy, in ECOSS the same channeling mechanism results in a background which is a smooth, monotonically decreasing function of energy. Calculations have shown that this background also cannot be described by the widely accepted background model AE^{-r}.

C. Angle-integrated EELS

For quantitative EELS analysis the most interesting signals are the inner-shell ionization edges occurring at energy losses around and above 100 eV, superimposed upon a monotonically decreasing background, from which they must be isolated by subtraction. In most cases the background is expressed as AE^{-r} whereby A and r are derived by fitting the preedge background with the aid of various algorithms. We give an example of this commonly adopted background model for Al in the energy-loss region of 200–800 eV.

Applying least-squares fitting we calculate the power index r as a function of the energy window in which the fitting is done (Fig. 4). As the width of the window increases the value of r increases linearly. For example, changing the width from 50 to 250 eV, a relative change in r is less than 3% for sample thickness $D_2=0.25$; for a four-times-thicker sample ($D_2=1$) the corresponding change in r would be less than 5%. This energy dependence of r, when neglected, causes erroneous estimates of the elemental composition of the sample.

In addition r is also a function of the collection angle, as demonstrated in Fig. 5 for a window width 50 eV located at 200-eV energy loss. But r changes by about 10% when the collection angle increases from 5 to 50 mrad. The angular dependence, however, is complicated by the three contributions, each having its own angle-energy relation. For example, the characteristic angles of multiple plasmon or core-loss scattering are proportional to the energy losses; in contrast, the angular distribution of Compton scattering peaks at finite angle. The elastic-

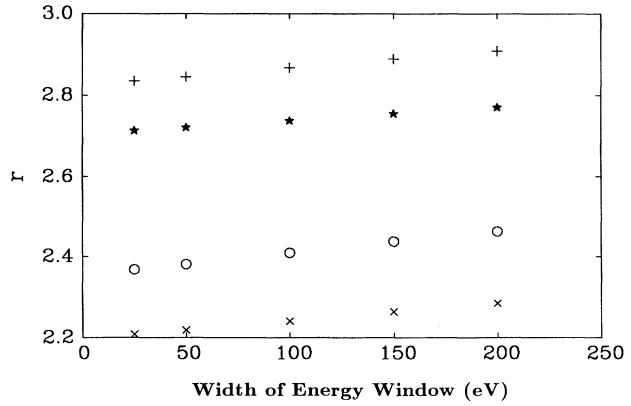

FIG. 4. Dependence of parameter r on the width of energy window located at $E=200$ eV. ×, $D_2=1$, $\alpha=15$ mrad; ○, $D_2=1$, $\alpha=5$ mrad; *, $D_2=0.25$, $\alpha=15$ mrad; +, $D_2=0.25$, $\alpha=5$ mrad.

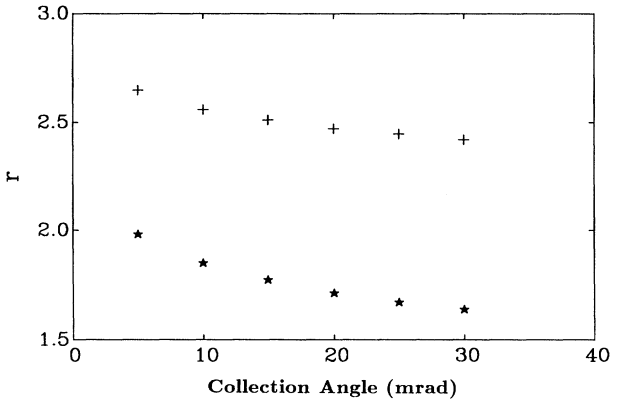

FIG. 5. Dependence of parameter r on the collection angle: *, $D_2=2$; +, $D_2=0.5$; energy window is 50 eV at 200-eV energy loss.

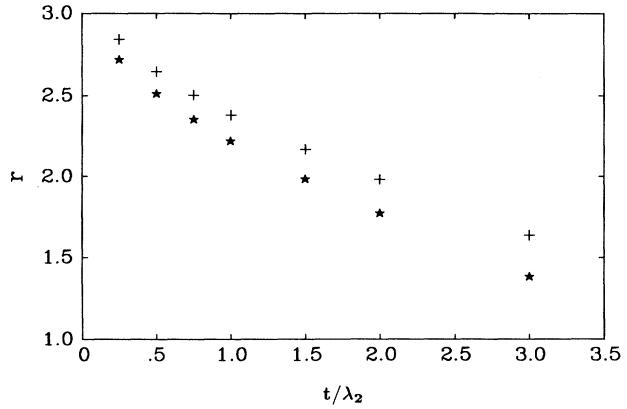

FIG. 6. Dependence of parameter r on specimen thickness D_2: $\alpha=15$ mrad; +, $\alpha=5$ mrad; energy window is 50 eV at 200-eV energy loss.

inelastic channeling becomes unpredictable as the thickness increases.[36]

Finally, most important is how multiple scattering of the electrons influences the free parameter r, i.e., how r depends on specimen thickness. The answer to this question can be seen in Fig. 6. In contrast to the other dependences discussed above, r shows a strong change with increasing sample thickness, which might result in faulty analyses when samples of inhomogeneous thickness are investigated.

In the light of these findings, the definition of an optimum thickness requires new discussion. Consideration of only single loss or triple loss[3,37] is obsolete. The method presented here permits a more exact estimation of optimum thickness.

VI. CONCLUSION

We present a complete analysis of the background in EELS. At large observation angles coupling from the elastic scattering channel to the inelastic one produces spurious plasmon peaks. In contrast, the background of electron Compton scattering decreases monotonically with increasing energy and angle. In neither case can the background be uniquely described by a power law.

For the case of angle-integrated EELS the background model AE^{-r} is unsuitable. The free parameter r is arbitrary, cannot be uniquely determined, and depends on collecting angle, width of energy window, and specimen thickness. The very strong dependence on specimen thickness restricts the application of the simple background model. This analysis explains why the results of EELS microanalysis are sensitive to the choice of the experimental settings, especially to the specimen thickness.[38]

ACKNOWLEDGMENT

D.S.S. thanks the Max-Planck Gesellschaft for financial support.

[1]H. Raether, *Excitation of Plasmons and Interband Transitions by Electrons* (Springer-Verlag, Berlin, 1980).
[2]R. F. Egerton, *Electron Energy-Loss Spectroscopy in the Electron Microscope* (Plenum, New York, 1986).
[3]M. Isaacson and D. Johnson, Ultramicroscopy **1**, 33 (1975).
[4]C. Colliex and B. Jouffrey, C. R. Acad. Sci. Paris **270**, 673 (1970).
[5]L. Reimer, I. Fromm, and I. Naundorf, Ultramicroscopy **32**, 80 (1990).
[6]B. G. William, M. P. Parkison, C. J. Eckhardt, and J. M. Thomas, Chem. Phys. Lett. **78**, 434 (1981).
[7]M. Inokuti, Rev. Mod. Phys. **43**, 297 (1971).
[8]D. R. Liu and D. B. Williams, *Proceedings of the 45th Annual Meeting of EMSA* (San Francisco Press, San Francisco, 1987), p. 118.
[9]P. Rez, *Microbeam Analysis-1979* (San Francisco Press, San Francisco, 1979), p. 117.
[10]R. D. Leapman and C. R. Swyt, *Microbeam Analysis-1983* (San Francisco Press, San Francisco, 1983), p. 163.
[11]B. Jouffrey, G. Zanchi, Y. Kihn, K. Hssein, and J. Sévely, Beitr. Elektronenmikroskop. Direktabb. Oberfl. **22**, 249 (1989).
[12]R. F. Egerton and Z. L. Wang, Ultramicroscopy, **32**, 137 (1990).
[13]D. S. Su, Ph.D. thesis, Technische Universität Wien, 1991.
[14]D. S. Su, P. Schattschneider, and P. Pongratz, Phys. Rev. B **46**, 2775 (1992).
[15]A. Crewe and T. Groves, J. Appl. Phys. **45**, 3668 (1974).
[16]L. Reimer, Ultramicroscopy **31**, 169 (1989).
[17]L. Landau, J. Phys. USSR **8**, 201 (1944).
[18]O. Blunck and S. Leisegang, Phys. **128**, 500 (1950).
[19]P. V. Vavilov, Zh. Eksp. Teor. Fiz. **32**, 920 (1957) [Sov. Phys. JETP **5**, 749 (1957)].
[20]P. Rez, Ultramicroscopy **12**, 29 (1983).
[21]T. Groves, Ultramicroscopy **1**, 15 (1975).
[22]E. Keil, E. Zeitler, and W. Zinn, Z. Naturforsch. Teil A **15**, 1031 (1960).
[23]P. E. Batson and J. Silcox, Phys. Rev. B **27**, 5224 (1983).
[24]P. Schattschneider, F. Foedermayr, and D. S. Su, Scanning Microsc. Suppl. **2**, 255 (1988).

[25]K. J. Krane, J. Phys. F **8**, 2133 (1978).
[26]F. Lenz, Z. Naturforsch. Teil A **9**, 185 (1954).
[27]B. Jouffrey, Ultramicroscopy **39**, 21 (1991).
[28]N. Sneddon, *Fourier Transforms* (McGraw-Hill, New York, 1951).
[29]H. F. Johnson, Comput. Phys. Commun. **43**, 181 (1987).
[30]H. F. Johnson and M. S. Isaacson, Ultramicroscopy **26**, 271 (1988).
[31]D. S. Su and P. Schattschneider, Philos. Mag. A **65**, 1127 (1992).
[32]D. S. Su, P. Jonas, and P. Schattschneider, Philos. Mag. B **66**, 405 (1992).
[33]D. L. Misell and R. E. Burge, J. Phys. C **2**, 61 (1969).
[34]P. Schattschneider, P. Pongratz, and H. Hohenegger, Scanning Microsc. Suppl. **4**, 35 (1990).
[35]B. Williams, *Compton Scattering* (McGraw-Hill, New York, 1977).
[36]D. S. Su, in *Proceedings of the 10th European Congress on Electron Microscopy* (Universidad de Granada, Granada, Spain, 1992), Vol. 1, p. 279.
[37]Y. Y. Wang, R. Ho, Z. Shao, and A. P. Somlyo, Ultramicroscopy **42**, 11 (1992).
[38]R. F. Egerton and S. C. Cheng, *Proceedings of the 50th Annual Meeting of the EMSA* (San Francisco Press, San Francisco, 1992), p. 1248.